

GT2011-46301

Numerical and Experimental Study of Polydispersed Acetone Spray Dispersion and Evaporation in Turbulent Flow

M. Chrighi

Institute for Energy and Power plant Technology, Department of Mechanical Engineering, TU Darmstadt, Petersenstr.30, 64287 Darmstadt, Germany

J. Gounder

Deutsches Zentrum für Luft- und Raumfahrt Pfaffenwaldring 38, 70569 Stuttgart, Germany

A. Sadiki

Institute for Energy and Power plant Technology, Department of Mechanical Engineering, TU Darmstadt, Petersenstr.30, 64287 Darmstadt, Germany

A. Masri

School of Aerospace, Mechanical and Mechatronic Engineering The University of Sydney, NSW 2006 Australia

ABSTRACT

Characteristics of acetone spray in a turbulent flow were numerically predicted and compared to experimental measurements. The focus was on the effect of polydispersity on the dispersion and evaporation of a relatively volatile fuel that featured a wide range of Stokes numbers in a turbulent two phase flow. Droplets were generated using an ultrasonic atomizer. It produced a relatively uniform velocity distribution with a moderate carrier to fuel velocities ratio. The simulations were performed in the framework of Reynolds Averaging Navier Stokes equations along with the Eulerian-Lagrangian approach where 12 different classes of the dispersed phase were tracked. Droplets differed in diameter, mean and rms velocities, and numbers density. The transport equations of the carrier phase were formulated in an Eulerian reference frame that included terms which accounted for the exchange of mass, momentum, energy and turbulence quantities with the spray, i.e. fully two way coupling. The phase transition was modeled by the Langmuir-Knudsen law that accounted for non equilibrium effects based on a consistent determination of the molar mass fraction on the droplet surfaces. Effects of turbulence modulation on the vaporization processes were resolved by a thermodynamically consistent model that determined the turbulence intensity at the droplet location, which affected the vapor concentration gradient near the droplet surfaces. For the droplet diffusion, the Markov sequence model was improved by adding a correction drift term to the fluid fluctuation velocity at the parcel position along the droplet trajectory. This correction term aimed at accounting for the non-homogeneity effects in

the turbulent flow. The different sub-models for the prediction of multiphase flow characteristics were applied to a 3D configuration that consisted of a spray nozzle mounted in a 4 m/s coflowing air stream. A number of carrier phase jet velocities were used, thus denoting a variation of the fuel to air mass loading. Radial profiles of the axial and radial velocities and its corresponding rms fluctuations of the acetone spray were predicted and compared to the experimental measurements. Spray mass flux, which determined the degree of evaporation, was plotted at different axial location from the nozzle exit plane. The study aimed at assessing the combination of different models applied to a mono-component spray for the prediction of two-phase flow and at investigating what should be improved for the case of real fuel (eg. Kerosene) for industrial configurations.

INTRODUCTION

Fuel injection as well as spray dispersion and evaporation in recently developed transport and power generation systems feature high potential for the optimization and reduction of gas emissions. These phenomena are sensitive to time and space uniformity of fuel vapor distribution. These time and space varying fuel properties (in the vapor and in liquid phase) affect substantially the vaporization and kinetics-related processes, like ignition, flame propagation/stability and pollutant levels. Crucial issues when designing a gas turbine combustor or IC-engine for liquid fuels are the understanding of flow-liquid interaction and the prediction of the mixture formation. Accurate modeling of these phenomena requires taking into account turbulence, heat transfer and fuel spray evaporation. The focus of this study is

on mechanisms and their interactions that are essential for the understanding of multiphase flows.

A lot of investigations and methods have been established to predict behaviour of the fuel spray, e.g. droplet dispersion, phase transition, mixing and combustion for single component sprays. Senoner et al. [1] investigated two phase flow with evaporating droplet using Large Eddy Simulation (LES) with different solvers, and compared the results to experimental data. They studied a complex geometry consisting of a swirl combustor fed with kerosene spray. The fuel was modeled by a single meta species. The simulation used a Uniform Temperature Model (UTM) for the evaporation. The coupling between both phases was achieved using source term within cells. Good results were shown for the velocities and corresponding velocities. Yet, no validations of the droplet diameters or liquid mass fluxes were provided. Apte et al. [2], performed numerical simulation to study evaporating spray in a coaxial combustor. They used collocated grid and incompressible algorithm to solve a hybrid particle-parcel and capture the dispersion, size distributions, and spray evolution by comparing it with the spray pattern from the gas turbine injector. Sommerfeld and Qiu [3] studied droplet properties in turbulent flow with an emphasis on the phase transition. A very useful experimental data-set for validation of numerical models for evaporating one component volatile fuel was provided with detailed boundary conditions. Bini and Jones [4], performed LES of an evaporating acetone spray, where a new model for the filtered evaporation rate of the droplet was applied to study the characteristics of acetone spray. The model formulation was shown to be capable of reproducing droplet dispersion accurately. Pera et al. [5], focused on the modeling of subgrid scale mixture fraction variance to predict evaporating two phase flow. Direct Numerical Simulation (DNS) was used for the validation of the source terms, hence the limitation at a very simple configuration. Kim and Sung [6], determined the effects of ambient pressure on evaporation of single droplet and sprays. Similar evaporation model was applied as the one used within this study. However simulations were restricted on the investigation of droplet characteristics without accounting for the flow field, i.e. one way coupling. Very recently, Bilger [7], addressed the modeling of mixture fraction formation and droplet evaporation. He suggested considering the fluctuation of temperature and species concentration beside those coming from the turbulent velocity fluctuation. Kristyadi et al [8] studied numerically and experimentally the evaporation and heating of mono-disperse mono-component droplets. A set of one component fuel with increasing molar mass were investigated. The modeling was extended to account for the internal recirculation inside the droplets and therefore an effective thermal conductivity model was adapted. Hence the discretization of the spray phase was needed, making the simulation of real configuration not achievable due to immense computational costs. Beside the above mentioned references, considerable outstanding work was addressed to assess phase transition and dispersion in two phase flow as well as mixture fraction formation. This work is auxiliary study where the effect of polydispersity and variable liquid to air mass-loading is investigated in a fully two-way coupling.

MATHEMATICAL MODELS AND NUMERICAL PROCEDURES

The approach adopted to solve the two-phase flow is based on a Eulerian-Lagrangian method. Droplets are described by a Lagrangian transport through a continuous carrier gas flow, which is captured by an Eulerian approach.

Governing Equations for Turbulent Gaseous Flow

The turbulent fluid phase is described following RANS-modeling approach. For this purpose, the transport equations have been solved for mass conservation, momentum, concentration and temperature, i.e. eq. (1)-(4).

$$\frac{\partial \bar{\rho}}{\partial t} + \frac{\partial (\bar{\rho} u_i)}{\partial x_i} = \bar{S}_{1,p,v}, \quad (1)$$

$$\frac{\partial (\bar{\rho} u_i)}{\partial t} + \frac{\partial (\bar{\rho} u_i u_j)}{\partial x_j} = \bar{\rho} g_i - \frac{\partial \bar{p}}{\partial x_i} + \quad (2)$$

$$\frac{\partial}{\partial x_j} \left(\mu \frac{\partial \bar{u}_i}{\partial x_j} - \overline{\rho u_i u_j} \right) + \bar{S}_{u_i,p,s} + \bar{S}_{u_i,p,v}$$

$$\frac{\partial (\bar{\rho} y)}{\partial t} + \frac{\partial (\bar{\rho} u_j y)}{\partial x_j} = \frac{\partial}{\partial x_j} \left(\bar{\rho} \Gamma \frac{\partial \bar{y}}{\partial x_j} - \overline{\rho u_j y} \right) + \bar{S}_{y,p,s} + \bar{S}_{y,p,v}, \quad (3)$$

$$\frac{\partial (\bar{\rho} T)}{\partial t} + \frac{\partial (\bar{\rho} u_j T)}{\partial x_j} = \frac{\partial}{\partial x_j} \left(\bar{\rho} \Gamma \frac{\partial \bar{T}}{\partial x_j} - \overline{\rho u_j T} \right) + \bar{S}_{T,p,s} + \bar{S}_{T,p,v}, \quad (4)$$

For the turbulence description, the *RNG* model which was adjusted for two-phase flows has been considered, i.e. eq. (5) and (6).

$$\frac{\partial k}{\partial t} + \frac{\partial (\bar{u}_i k)}{\partial x_i} = \frac{\partial}{\partial x_i} \left(\frac{\nu_t}{Pr_k} \frac{\partial k}{\partial x_i} \right) - \overline{u_i u_j} \frac{\partial \bar{u}_j}{\partial x_i} - \varepsilon + \bar{S}_{k,p,s} + \bar{S}_{k,p,v} \quad (5)$$

$$\frac{\partial \varepsilon}{\partial t} + \frac{\partial (\bar{u}_i \varepsilon)}{\partial x_i} = \frac{\partial}{\partial x_i} \left(\frac{\nu_t}{Pr_\varepsilon} \frac{\partial \varepsilon}{\partial x_i} \right) - C_{\varepsilon 1} \frac{\varepsilon}{k} \overline{u_i u_j} \frac{\partial \bar{u}_j}{\partial x_i} - \quad (6)$$

$$\left(C_{\varepsilon 2} + \frac{C_\mu \eta^3 (1 - \eta/\eta_0)}{1 + \beta \eta^3} \right) \frac{\varepsilon^2}{k} + \bar{S}_{\varepsilon,p,s} + \bar{S}_{\varepsilon,p,v}$$

where

$$\eta = S \frac{k}{\varepsilon} \quad (7)$$

The variables μ , Γ , S , and Pr denote the viscosity, diffusivity, magnitude of the vorticity and the turbulent Prandtl number respectively. The quantities η_0 , $C_{\varepsilon 1}$, $C_{\varepsilon 2}$ and β are model constants. The influence of the dispersed phase on the fluid motion is treated as an extra force exerted on the carrier gas. Thus, the momentum transfer from the dispersed phase to the carrier phase is included by adding a reaction force to the Navier-Stokes equations which acts as a surface force on the droplet. This model is known as force coupling model or particle-source-in-cell (PSI-Cell) model proposed by Crowe et al. [10]. The source terms $\bar{S}_{\psi,p,s}$ and $\bar{S}_{\psi,p,v}$ that characterize the direct interaction of mass, momentum, turbulence, energy and species between the droplets and the carrier gas are given in detail in [9] and [12].

Droplet Evaporation and Dispersion Models

As pointed out above, a Lagrangian approach is employed to compute properties of droplets moving in turbulent flow. Trajectories of various droplet classes are obtained from motion equations, where all external effects except drag,

buoyancy and gravity forces are neglected. In order to quantify the instantaneous fluid velocity seen by the droplets and its effect on the droplet dispersion, one should model the Root Mean Square (RMS) values of the fluid parcel velocity at the droplet location. In fact this is a key question of the dispersed phase flow modeling, namely the description of the fluid turbulence along the droplet trajectories. This can be adequately done using a stochastic Lagrangian process, in terms of the computed fluid turbulent variables to generate the instantaneous fluid velocity in the discrete droplet dynamic equation. Droplet and fluid element have the same temporal t_n and spatial location. After one time step Δt , the droplet and fluid element change their positions. However, they do not overlap because of drag and external forces acting on the droplet. The Markov sequence model is based on the following two steps for the computation of the fluid element fluctuation along the droplet trajectory:

- The evolution of the fluid element velocity fluctuation along the stream line is determined using the Lagrangian correlation factor:

$$u_{i,F}^{\prime F}(t_{n+1}) = u_{i,F}^{\prime F}(t_n) \cdot R_{L,i}(\Delta t) + \sigma_i \sqrt{1 - R_{L,i}^2(\Delta t)} \cdot \zeta_i(t_n) \quad (8)$$

- The fluid element velocity fluctuation located at the droplet position $u_{i,p}^{\prime F}$ is correlated with the fluid element location using the Eulerian correlation factor:

$$u_{i,p}^{\prime F}(t_{n+1}) = u_{i,F}^{\prime F}(t_{n+1}) \cdot R_{E,i}(\Delta r) + \sigma_i \sqrt{1 - R_{E,i}^2(\Delta r)} \cdot \zeta_i(t_n) \quad (9)$$

The Lagrangian and Eulerian correlation factors defined by equations (10) and (11) denote the time and spatial correlation functions respectively.

$$R_{L,i}(\Delta t) = \frac{\overline{u_{i,F}^{\prime F}(t) u_{i,F}^{\prime F}(t + \Delta t)}}{\sqrt{\overline{(u_{i,F}^{\prime F}(t))^2}} \sqrt{\overline{(u_{i,F}^{\prime F}(t + \Delta t))^2}}}, \quad (10)$$

$$R_{E,i}(\Delta r) = \frac{\overline{u_{i,F}^{\prime F}(r) u_{i,p}^{\prime F}(r + \Delta r)}}{\sqrt{\overline{(u_{i,F}^{\prime F}(r))^2}} \sqrt{\overline{(u_{i,p}^{\prime F}(r + \Delta r))^2}}}. \quad (11)$$

The product of both correlation factors (Lagrangian $R_{L,i}(\Delta t)$ and Eulerian $R_{E,i}(\Delta r)$) yields to a new coefficient which can be used to compute the fluctuation of the fluid element at the droplet location [15]:

$$R_{p,i}(\Delta t, \Delta r) = R_{L,i}(\Delta t) \cdot R_{E,i}(\Delta r), \quad (12)$$

$$u_{i,p}^{\prime F}(t_{n+1}) = u_{i,p}^{\prime F}(t_n) \cdot R_{p,i}(\Delta t, \Delta r) + \sigma_i \sqrt{1 - R_{p,i}^2(\Delta t, \Delta r)} \cdot \chi_i(t_n) \quad (13)$$

Turbulent flows are rather not homogenous in many configurations. Thus the flow develops stress gradients which are responsible for the enhancement of the pressure gradient. Therefore, droplets are immigrating to locations having low pressure, i.e. low turbulent intensity. To avoid these phenomena in the frame of the Markov-sequence dispersion model used in this work, a drift correction term has to be considered [16].

The final expressions for the fluid fluctuations at droplet location (fluctuation seen by dispersed phase) are then calculated by:

$$u_p^{\prime F}(t_{n+1}) = u_p^{\prime F}(t_n) \cdot R_{p,u}(\Delta t, \Delta r) + \sigma_u \sqrt{1 - R_{p,u}^2(\Delta t, \Delta r)} \cdot \zeta_u(t_n) \quad (14)$$

$$+ (1 - R_{p,u}(\Delta t, \Delta r)) T_{L,u} \frac{\partial u^{\prime F}}{\partial x}$$

$$v_p^{\prime F}(t_{n+1}) = v_p^{\prime F}(t_n) \cdot R_{p,v}(\Delta t, \Delta r) + \sigma_v \sqrt{1 - R_{p,v}^2(\Delta t, \Delta r)} \cdot \zeta_v(t_n) \quad (15)$$

$$+ (1 - R_{p,v}(\Delta t, \Delta r)) T_{L,v} \frac{\partial v^{\prime F}}{\partial y}$$

$$w_p^{\prime F}(t_{n+1}) = w_p^{\prime F}(t_n) \cdot R_{p,w}(\Delta t, \Delta r) + \sigma_w \sqrt{1 - R_{p,w}^2(\Delta t, \Delta r)} \cdot \zeta_w(t_n) \quad (16)$$

$$+ (1 - R_{p,w}(\Delta t, \Delta r)) T_{L,w} \frac{\partial w^{\prime F}}{\partial z}$$

where $\zeta_u(t_n)$, $\zeta_v(t_n)$ and $\zeta_w(t_n)$ note Gaussian random variables. For the Lagrangian correlation factor, an exponential approach was considered:

$$R_{L,i}(\Delta t) = \exp\left(-\frac{\Delta t}{T_{L,i}}\right), \quad (17)$$

where $T_{L,i}$ represents the Lagrangian integral time scale as it is calculated for RNG turbulence model by $T_{L,i} = c_T k / \varepsilon$. When using Reynolds stress models, $T_{L,i}$ is determined (for all direction, x , y and z) by:

$$T_{L,i} = c_T \frac{\sigma_i^2}{\varepsilon}, \quad (18)$$

where the constant c_T equals 0.3 and σ_i^2 denotes $\overline{u_i^{\prime F} u_i^{\prime F}}$. The Eulerian correlation factor $R_{E,i}(\Delta r)$ is computed using longitudinal and transversal correlation functions $f(\Delta r)$ and $g(\Delta r)$ according to [17].

$$R_{E,i}(\Delta r) = (f(\Delta r) - g(\Delta r)) \frac{\Delta r_i \Delta r_j}{\Delta r^2} + g(\Delta r) \delta_{ij} \quad (19)$$

The longitudinal and transversal correlations functions $f(\Delta r)$ and $g(\Delta r)$ are computed using the following expression:

$$f(\Delta r) = \exp\left(-\frac{\Delta r}{L_E}\right) \quad (20)$$

$$g(\Delta r) = \left(1 - \frac{\Delta r}{2L_E}\right) \exp\left(-\frac{\Delta r}{L_E}\right), \quad (21)$$

where L_E represents a simplified turbulent length scale which is determined by:

$$L_E = c_L T_L \sigma. \quad (22)$$

T_L is computed according to equation (18) and c_L represents a model constant set to 3.0 as given in [18].

For the phase transition, two additional equations which give the rate of change of droplet diameter and temperature with respect to time are needed (e.g. [12] and [13]).

To account for the 3D-evaporation of droplets, a non-equilibrium model [14] was considered. This model is based on the film thickness theory. It does not consider any temperature variation in the interior of the droplet (homogenous temperature). However, the temperature variation has an unsteady behavior and is accompanied with an unsteady mass transition. As this model does not account for the gradients at the droplet interior, it is therefore not discretized. Thus, this model does not require high computing time. In order to reduce the

complexity of the theoretical description the following basic assumptions and simplifications are made.

- Droplets are assumed to be spherical.
- Secondary atomization and coalescence of droplets are neglected since the region that the simulations are related with features a dilute spray i.e. simple elastic collisions between droplets and wall are assumed without any kind of film formation.
- The influence of the surface tension is neglected, i.e. a uniform pressure around the droplet is assumed.
- Uniform physical properties of the surrounding fluid and liquid-vapor thermal equilibrium on the droplet surface.
- The ambient air is not soluble in the droplet fluid.
- Chemical reactions are not considered
- Radiation has no effect on the evaporation, since the acetone boiling temperature equals 330 K that yields negligible heat loss due to radiation.

The evaporation model describes the evolution of the droplet temperature and diameter, i.e. evaporation rate and energy flux through the liquid/gas interface.

The vaporization rate is calculated by considering the mass transfer around the droplet following Park et al [20] and Berlemont et al [19].

$$\dot{m}_{p,v} = 2\pi r_p \overline{\rho_m} \overline{D_m} Sh^* \frac{\ln(1+B_M)}{B_M} \quad (23)$$

where r_p is the droplet radius, $\overline{\rho_m}$ and $\overline{D_m}$ are the averaged values of the mixture density and binary diffusion coefficient throughout the film, respectively. B_M represents the Spalding's mass transfer number defined by

$$B_M = \frac{y_s - y_\infty}{1 - y_s}, \quad (24)$$

in which y_s is the surface vapor mass fraction and y_∞ is the vapor mass fraction far from the droplet. In particular y_s depends on the vapor relative pressure which itself depends on the droplet surface temperature.

$$y_s = \frac{\chi_{s,neq}}{\chi_{s,neq} - (1 - \chi_{s,neq})\theta_2} \quad (25)$$

where θ_2 is the ratio of molecular weights. Non equilibrium effects were captured by determining the departure from thermodynamic equilibrium by adding a deviation term to the molar fraction of the vapor at the droplet surfaces, which is expressed as:

$$\chi_{s,neq} = \chi_{s,eq} - \left(\frac{L_K}{d/2} \right) \beta_L \quad (26)$$

where

$$\beta_L = - \left(\frac{3Pr_G \tau_d}{2} \right) \frac{\dot{m}}{m}, \quad (27)$$

which represents the half of the blowing Peclet number. d is the droplet diameter, Pr_G is the Prandtl number, L_K represents the Knudsen length and τ_d is the particle relaxation time. The variable $\chi_{s,neq}$ represents the molar fraction in case of

equilibrium state. It is determined using the saturation pressure through the Clausius-Clapeyron equation. The accuracy of the evaporation rate depends strongly on the determination of the values of $\overline{\rho_m}$ and $\overline{D_m}$. The physical properties of the air vapor mixture (in the gaseous film around the droplet) are determined using the reference temperature and mass fraction. They are calculated using the Simpson or Sparrow & Gregg "1/3 rule", see Berlemont et al [19], from which the best accuracy of these quantities have been obtained. The droplet radius is obtained from the equation of the diameter evolution for each droplet by:

$$\frac{dD_p}{dt} = - \frac{2\dot{m}_{p,v}}{\pi\rho_L D_p^2} - \frac{D_p}{3\rho_L} \frac{\partial\rho_L}{\partial T_p} \frac{dT_p}{dt}, \quad (28)$$

where ρ_L is the liquid density, D_p the droplet diameter and T_p the droplet temperature. The effects of convection on the vaporization and the heat flux rate are taken into account by means of semi-empirical correlations such as those for the drag coefficient, the Sherwood number and the Nusselt number.

The quantity Sh^* in eq. (23) denotes the modified Sherwood number which includes the effects of the Stefan flow. It is defined by

$$Sh^* = 2 + \frac{Sh_0 - 2}{F_M} \quad (29)$$

where Sh_0 is given in eq. (30), see Clift et al. (1978 pp. 49), represents the Sherwood number in case of negligible evaporation, i.e. the Stefan flow is not accounted for.

$$Sh_0 = 1 + (1 + Re_p Sc_p)^{1/3} f(Re_p) \quad (30)$$

Re_p is the droplet Reynolds number and Sc_p is the Schmidt number while $f(Re_p)$ is an empirical function defined as:

$$f(Re_p) = Re_p^{0.077}. \quad (31)$$

The function F_M represents a correction factor, which takes into consideration the relative change of the mass film thickness due to the droplet evaporation process [25]:

$$F_M = F_M(B_M) = (1 + B_M)^{0.7} \ln \left(\frac{1 + B_M}{B_M} \right). \quad (32)$$

The evaporation is coupled with the droplet energy/heating in (28) where the droplet temperature variations is described by

$$\frac{dT_p}{dt} = - \frac{6\dot{Q}_l}{\rho\pi c_{pL} D_p^3}, \quad (33)$$

where c_{pL} denotes the heat capacity coefficient of the liquid and \dot{Q}_l the heat flux rate penetrating into the droplet. The latter is calculated similarly to the evaporation rate and related to it by:

$$\dot{Q}_l = \dot{m}_{p,v} \left(\frac{c_{pm}(T_\infty - T_p)}{B_T} - h_v(T_p) \right), \quad (34)$$

where $h_v(T_p) = r(T_p) + \dot{Q}_l / \dot{m}_{p,v}$ expresses the effective latent heat of vaporization. It is a function of temperature and varies with the considered liquid. $r(T_p)$ is the true latent heat of

The simulations were performed using 12 different classes of droplets. Figure 2 shows the Probability Density Function of the droplet number for each class. Droplets having diameter higher than 80 μm yield negligible number, yet their mass flow rate is important. This is due the correlation of droplet mass with the cube of the diameter, e.g. three times bigger droplets contain 27 times more mass. Figure 3 shows the mass flow rate distribution for each droplet class. Giving exact BC for the classes with $d_p > 80 \mu\text{m}$ is extremely crucial for the dispersed phase properties. Indeed larger droplets endure longer travel distances.

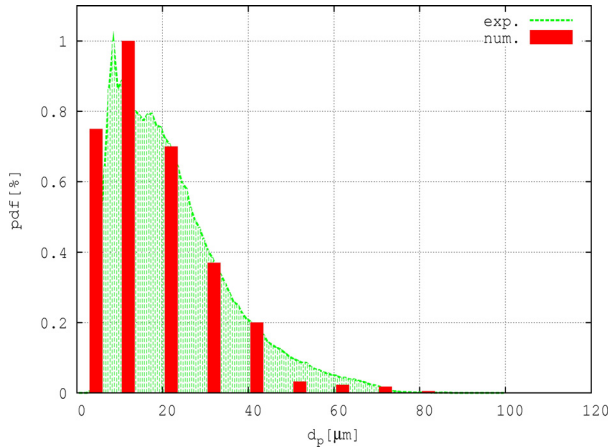


Figure 2: PDF of the droplet number. Num. BC vs. exp.

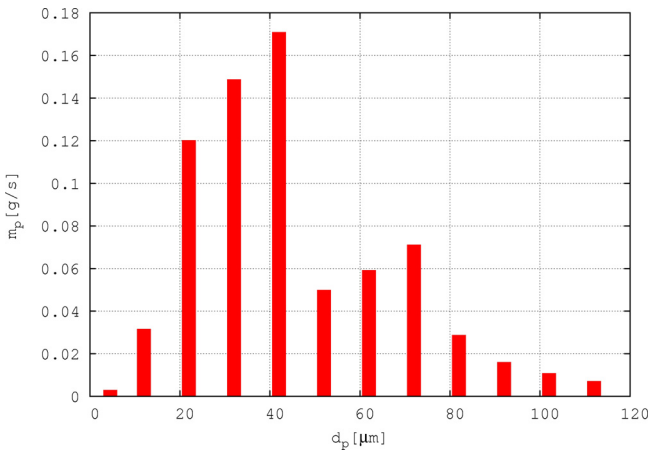


Figure 3: Mass flow rate distribution per class

Figure 2 shows the distribution of the droplet classes, given numerically, and compared to the experimental data measured for case Sp8. Figure 4 shows the axial droplet velocity and its fluctuations. The mean axial velocity for all droplet classes is 42 m/s, whereas the standard deviation corresponds to approximately 3 m/s yielding an axial turbulence intensity of 7.5%. The radial component is shown in Figure 5. The radial velocity, v_p , is less than 2.5 m/s and goes to zero at the axis because of the symmetry condition. The fluctuation, v'_p , is more important if compared to v_p .

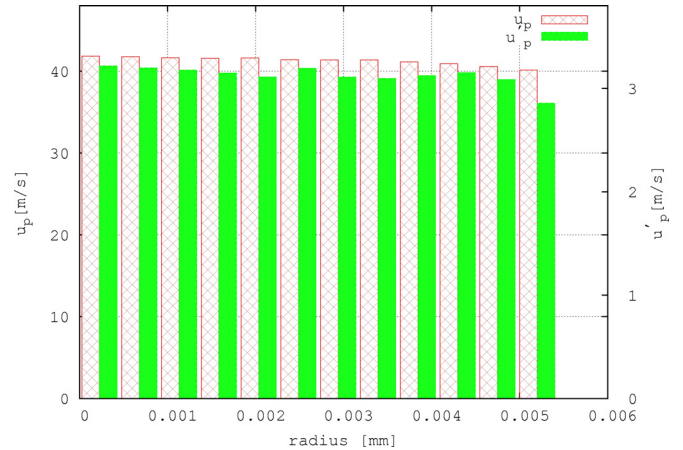


Figure 4: Axial droplet velocity and its fluctuations.

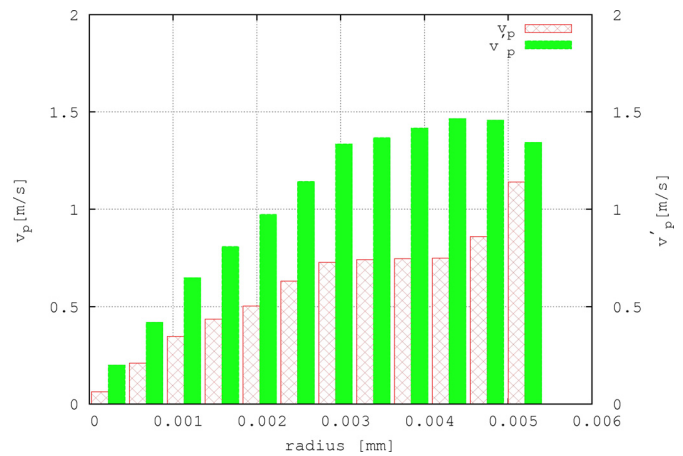


Figure 5: Radial droplet velocity and its fluctuations.

The computational domain consists of 17 blocks that count 553774 control volumes. The total number of the numerically tracked droplets exceeded 1 million parcels within one coupling-iteration, thus the results are proven to be consistent, since an augmentation of the number of parcels or a refining of the computational domain has not improved or changed the numerical profiles, which means statistically independent results. The profiles of the droplet characteristics feature PDF moments that are not conditioned by the droplet number within the control volume. The convergence of the Eulerian-Lagrangian coupling procedure is reached when the fluids' properties do not change their value from one coupling to the next in the presence of droplets. Unfortunately, there are no universal guidelines for selecting criteria because they depend not only on the physical processes being approximated but also on the details of the numerical formulation. Kohnen et al. [26] studied the convergence of Euler-Lagrange approach. They found that the normalized residuals were not suitable for use as a criterion for the convergence of the coupling due to the oscillation that follows each source term transfer. They suggested that the evolution of the gas phase velocity profiles at several reference positions should be used as a convergence criterion. In this work, the interaction between both phases is considered converged when the radial profiles of the carrier

phase at considered measurement locations remain unchanged from one coupling to the following one.

NUMERICAL PROCEDURE

The dispersed phase is tracked using the academic Lagrangian code LAG3D, whereas the carrier phase was solved with the three dimensional code, LAFTEST 3D, in which the equations for the gas phase are solved by finite volume method. The time integration is achieved implicitly with the Crank-Nicholson method, the diffusion terms are discretized with central schemes on a non orthogonal block-structured grid. The velocity-pressure coupling is accomplished by a SIMPLE algorithm. The whole system is solved by the SIP-solver. The Lagrangian equations for droplets are discretized using first order scheme and solved explicitly. Source terms for the gas phase are computed in each cell with contributions from all the relevant droplets.

Numerically, the interaction between the continuous and the dispersed phases consists in couplings between two modules involved. The coupling between the continuous and disperse phases is achieved using the force coupling model known as the particle-source-in-cell (PSI-Cell) model proposed by Crowe et al.[24].

After several iterations of gas phase alone, the gas variables are kept frozen and all the droplets representing the entire spray are injected in the computational domain. High levels of under-relaxation factors were used on all gas variables in order to obtain successful convergence. Due to the presence of droplets source terms, the conventional residuals are characterized by a jump of residuals after each coupling. To avoid divergence, an additional under-relaxation technique should also be employed for droplet source terms.

$$S_{\phi_p}^{i+1} = S_{\phi_p}^i \cdot (1 - \gamma) + S_{\phi_p(cal.)}^{i+1} \cdot \gamma, \quad (43)$$

where $S_{\phi_p}^i$ and $S_{\phi_p}^{i+1}$ are the particle source terms appearing at $(i+1)$ -th and i -th couplings, respectively. The under-relaxation factor γ , takes values in the range $[0,1]$.

The droplet injection is based on a stochastic approach by considering the droplet mass flux and the droplet size distributions obtained at the inlet near the nozzle exit from experimental measurements.

The numerical interaction between both phases, i.e. between the Euler code and the Lagrange, for the configuration under study needed 10 couplings for each test case. The computational time is 10 h per CPU for each coupling.

RESULTS AND DISCUSSION

The droplet axial velocities of the three test cases are plotted in Figure 6. Very good agreement between numerical prediction and experimental measurements is observed. The velocity curves feature a smooth profile hinting to statistically independent results, i.e. the number of numerical parcels used within each coupling reveals enough samples to deliver mean velocities that are independent to the injected parcels. The increase of the jet velocity maximums for the test cases Sp3 to Sp8 is due to the augmentation of the carrier phase mass flux at the boundary conditions. Figure 7 exhibit the fluctuation of the droplet axial velocity at different axial distance ($x/D=0.3$

to $x/D=30$) from the nozzle exit plane. Discrepancies are observed close to the nozzle exit, where the spray air flow is relatively dense. Both experimental and numerical results may demonstrate elevated error range. The measurement of droplet properties in dense regions and close to the nozzle exit is very complex and associated with high uncertainties. The numerical simulations could also be affected due to models for parcel-parcel or/and parcel-wall interactions being not considered. The under-prediction of the axial velocity second moment is correlated with the detachment of the spray from the nozzle edge and the droplet acceleration, which is dependent on their diameter. Overall the numerical prediction captures the trends shown in the experimental results well. At the nozzle exit plane, the fluctuation profiles featured a maximum, which is derived from the high gradient of the axial velocity seen in the shear flow. These high gradients in the shear zone play the role of a source for enhancing the second moment. The spray interaction with the nozzle edge at the exit may favor the fluctuation, namely film ligaments that were experimentally observed, however they were not accounted for numerically. These ligaments yield different classes of droplets that would be dragged and accelerated according to their diameter and form. Further downstream, a good agreement between predicted results and the experimental data is achieved.

Figures 8 and 9 illustrate the radial mean velocity profiles and its fluctuations respectively, at different distances from the nozzle exit plane. Regions viewing a zero velocity, e.g. toward the co-flow, are caused by the absence of the disperse phase. Cells of the computational domain that contain no droplets display zero values for the dispersed phase properties. The profiles demonstrate small discrepancies which are within the experimental error range. The magnitude for both, i.e. mean velocities and fluctuations, show an increasing trend from Sp3 to Sp8 which is explained by the different inlet mass flux of the carrier phase.

It is worth mentioning that the fluctuations are of the same order of magnitude as the mean values. The radial velocity at $x/D=0.3$ is negligible because of the interaction with the nozzle edge. Further downstream, the spray is distributed more homogenously, and the droplets disperse horizontally yielding a uniform profile. From the former four figures, it is shown that the dynamics of the dispersed phase is well predicted in the axial and radial directions. The dispersion model should be further investigated with respect to the dense two-phase flow. Moreover, the droplet formation and coalescence effects should be considered at this dense region.

Figure 10 shows the predicted arithmetic droplet mean diameter compared to the experimental data. The profiles of all test cases are similar and seem not to be explicitly affected by the augmentation of the carrier phase axial velocity. The droplet mean diameter remained almost constant while the spray was being carried downstream. This can be explained by the diversity of the disperse phase classes, which feature different evaporation rates, so that the statistics over all parcels within a control volume yield an unchangeable arithmetic mean diameter. This is, indeed, an indication that polydispersity is very well predicted and the evaporation of different classes is consistent. Masri and Gounder [27]

presented the droplet size distributions per droplet class, which gave an indication about the phase transition. However, the evaporation rate for each class could not be determined experimentally, since droplets that form a considered class which were recorded in one measuring cross section cannot be exactly identified later.

In Figure 11, the volume flux of the spray is plotted and compared to the experimental measurements at different distances from the nozzle exit plane. This parameter (α) is an indicator of the evaporation process. The volume flux is increasing from Sp3 to Sp8 as the carrier phase velocity is increased accordingly. While increasing their velocity, the droplets have less time to release their vapor in the environment, thus the liquid mass flux increase. The spray is completely evaporated beyond $x/D=30$. The predicted volume flux at $x/D=0.3$ for the Sp3 test case is over predicted compared to the experimental data. This could be due to droplet detachment effect from nozzle edge. Close to this region, droplets are not necessarily spherical, their interaction with the wall make their capture, experimentally, coupled with high error level.

The influence of turbulence modulation on the evaporation was presented by Sadiki et al in [28], see Figure 12. Therein, the authors highlighted the importance of a correct turbulence description using a consistent turbulence source terms and their effects on the phase transition. It was also shown that non-equilibrium evaporation model had produced better results in predicting the evaporation rate than the equilibrium one. The configuration used in the mentioned investigation consisted of a spray issuing into a co-flowing heated air-stream which is very similar to the one studied in this framework.

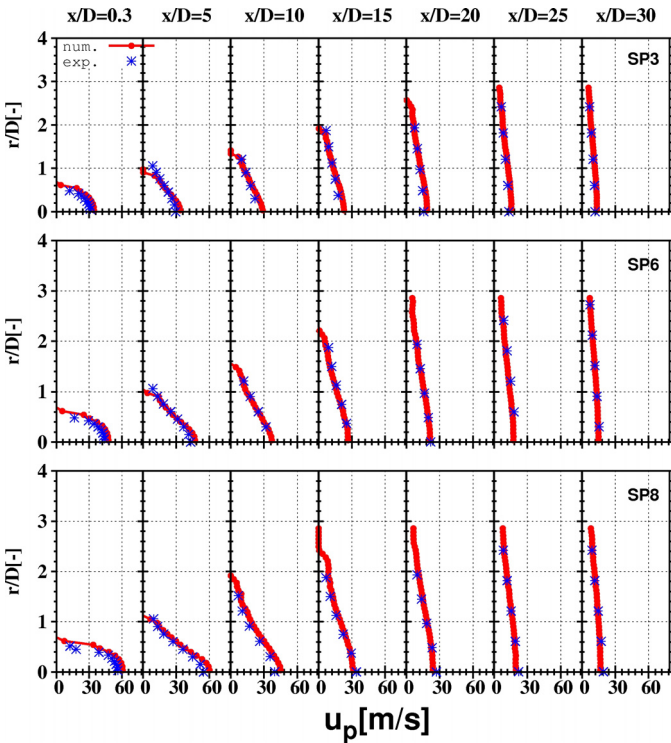


Figure 6: Droplet axial mean velocity for different loading (Sp3, Sp6 and Sp8) in [m/s]

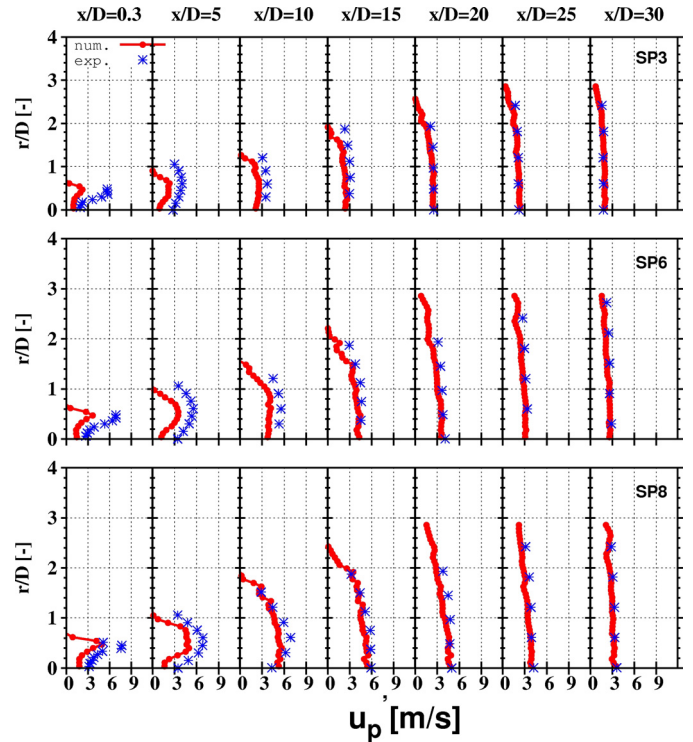


Figure 7: Droplet axial velocity fluctuations at different distances from the nozzle exit plane [m/s].

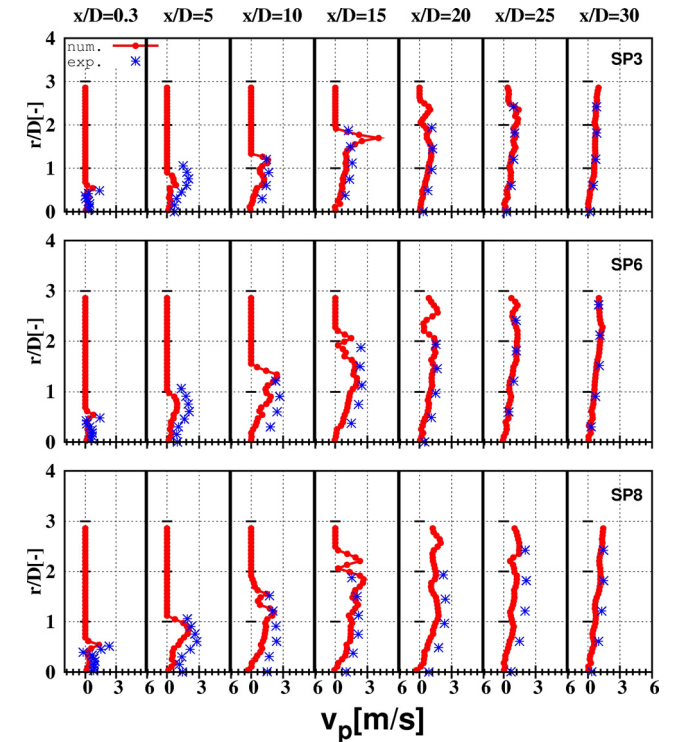


Figure 8: Droplet radial mean velocity profiles at different distances from the nozzle exit plane for diff. loadings [m/s]

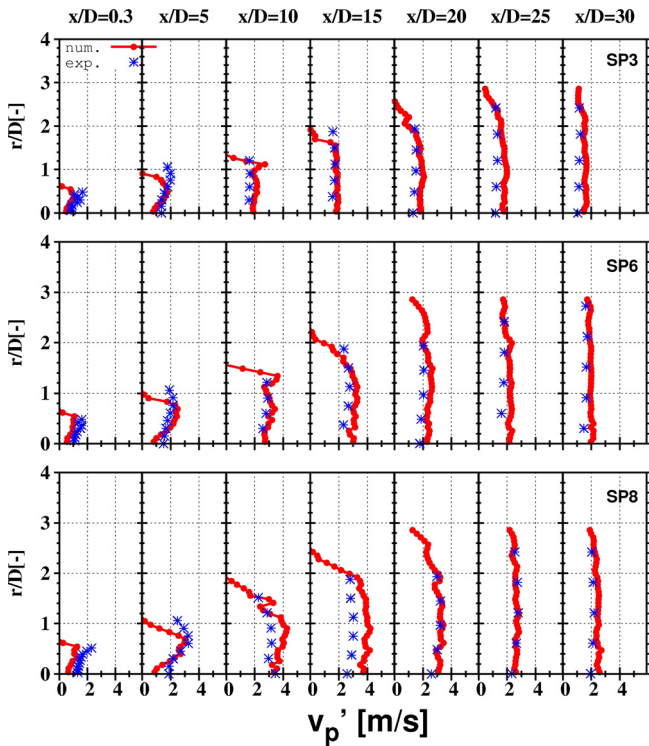


Figure 9: Droplet radial velocity fluctuations profiles at different distances from the nozzle exit plane for all loadings [m/s]

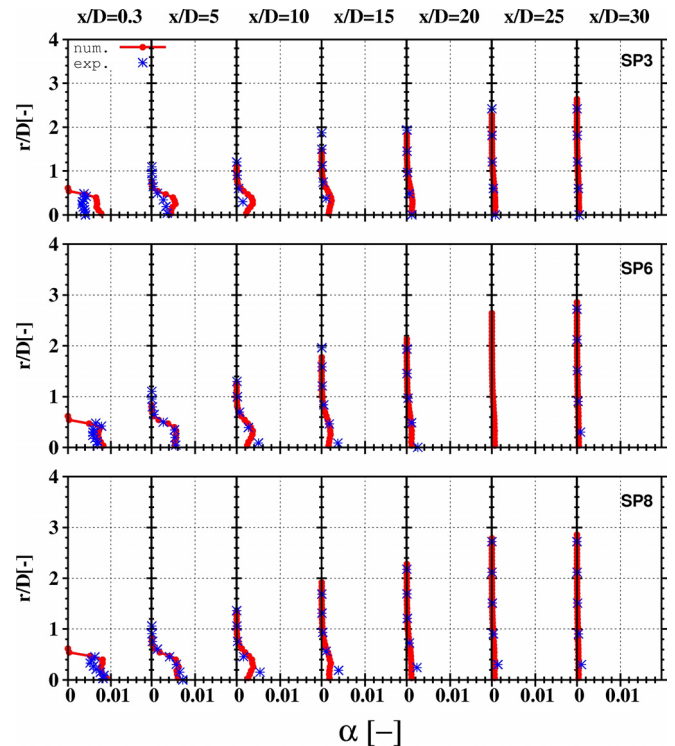


Figure 11: Spray volume flux for all loading at different distance from the nozzle exit plane [$\text{m}^3/(\text{m}^2 \cdot \text{s})$]

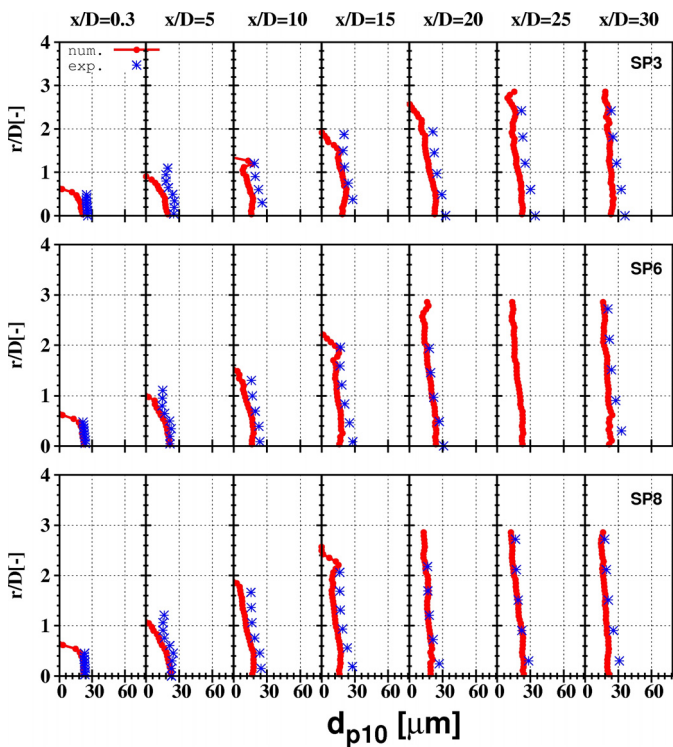


Figure 10: Droplet arithmetic mean diameter [μm]

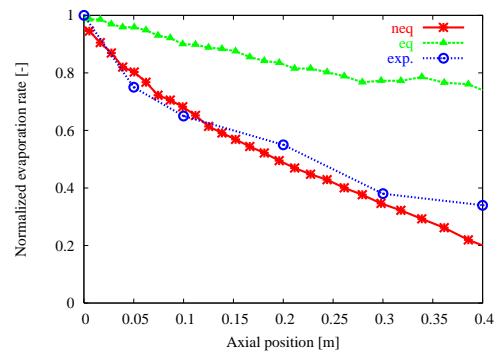


Figure 12: Normalized evaporation rate: Comparison between Equi. and Non equi. evaporation models [28].

CONCLUSION

Acetone spray properties of evaporating droplets were studied and plotted vs. experimental data. Good agreements were observed for the mean axial and radial velocities, however small discrepancies were noticed for the second moments, which were correlated to the spray interaction with the nozzle edge. The global model for the two phase flow, including sub-models for the evaporation, dispersion, turbulence modulation, polydispersity and fully two-way coupling delivered very promising results demonstrating the ability of the spray prediction, which play a major role for prediction of mixture formation and preparation. The phase transition, captured using the non-equilibrium evaporation model, and observed as the liquid volume flux, featured plausible agreement with experimental data. The computational time of 10 CPU hours / (500 000 cells x 1 Million parcels) per coupling between both phases is attractive for industrial applications. Further

investigations should be put on the wall spray interaction and the droplet formation as well as four way coupling at the dense flow region, e.g. close to the nozzle exit.

Acknowledgments

The authors acknowledge the financial support from the Deutsche Forschungsgemeinschaft (DFG) through the SFB568.

REFERENCES

- [1] J. M. Senoner, M. Sanjosé, T. Lederlin, F. Jaegle, M. García, E. Riber, B. Cuenot, L. Gicquel, H. Pitsch, T. Poinso "Eulerian and Lagrangian Large-Eddy Simulations of an evaporating two-phase flow" *Comptes Rendus Mécanique*, 337 458-468, (2009)
- [2] S. V. Apte, K. Mahesh, P. Moin: "Large-eddy simulation of evaporating spray in a coaxial combustor" *Proceedings of the Combustion Institute*, Volume 32, Issue 2, pp 2247-2256, (2009).
- [3] M. Sommerfeld, H. -H. Qiu: "Experimental studies of spray evaporation in turbulent flow" *Int. J. Heat Fluid Flow*, Issue 19 pp 10-22, (1998).
- [4] M. Bini, W.P. Jones "Large Eddy Simulation of an evaporating acetone spray" *International Journal of Heat and Fluid Flow*, Volume 30, Issue 3, pp 471-480, (2009).
- [5] C. Pera, J. Réveillon, L. Vervisch, P. Domingo "Modeling subgrid scale mixture fraction variance in LES of evaporating spray Combustion and Flame, Volume 146, Issue 4, pp 635-648, (2006).
- [6] H. Kim and N. Sung, The effect of ambient pressure on the evaporation of a single droplet and a spray, *Combustion and Flame*, Volume 135, Issue 3, Pages 261-270, (2003).
- [7] R. W. Bilger, A mixture fraction framework for the theory and modeling of droplets and sprays, *Combustion and Flame*, doi:10.1016/j.combustflame.2010.08.008, (2010).
- [8] T. Kristyadi, V. Deprédurand, G. Castanet, F. Lemoine, S.S. Sazhin, A. Elwardany, E.M. Sazhina and M.R. Heikal, Monodisperse monocomponent fuel droplet heating and evaporation, *Journal of Fuel*, Volume 89, Issue 12, Pages 3995-4001, (2010).
- [9] M. Chrigui, A. Sadiki, J. Janicka, M. Hage, A. Dreizler Experimental and numerical analysis of spray dispersion and evaporation in a combustion chamber, *Atomization and Sprays*, 19(10):929-955, (2009).
- [10] C. T., Crowe, M. P. Sharma, & D. E. Stock, The particle-source-in-cell (PSICELL) model for gas-droplet flows. *ASME Trans. J. Fluids Eng.* June. (1977).
- [11] M. Chrigui, G. Ahmadi, and A. Sadiki, "Study on Interaction in Spray between Evaporating Droplets and Turbulence Using Second Order Turbulence RANS Models and a Lagrangian Approach, " *Progress in Computational Fluid Dynamics*, (2004).
- [12] M. Chrigui, "N-Hpetane spray evaporation and dispersion in turbulent flow within a complex geometry configuration" *J. of computational thermal science* J. of computational thermal science, Vol. 2, Issue 1, pp 55-78, (2010).
- [13] B. Abramzon, B., W.A. Sirignano, "droplet vaporization Model for Spray Combustion Calculations," *Int. J. Heat Mass Transfer*, 32, pp. 1605-1618, (1989).
- [14] R. S. Miller, K. Harstad, and J. Bellan, "Evaluation of equilibrium and non-equilibrium evaporation models for many-droplet gas-liquid flow simulations," *Int. Journal of Multiphase Flow* 24, pp. 1025-1055, (1998).
- [15] M. Sommerfeld, "Modellierung und numerische Berechnung von partikelbeladenen turbulenten Strömungen mit Hilfe des Euler/Lagrange-Verfahrens." *Shaker Verlag Aachen*. ISBN 3-8265-1951-5, (1996).
- [16] M., Sommerfeld, H.H., Qiu, M., Rüger, G., Kohnen, P.J., Spies, D., Müller, "Spray evaporation in turbulent flow", *Proceedings of the 2nd Int. Symp. on Engineering Turbulent Modeling and Measurements*, Florence, Italy, 31 May - 2 June, pp. 935-945, (1993).
- [17] Th. Karman And L. Howarth, "On the statistical theory of isotropic turbulence", *Proc. Roy. Soc. London*, Vol. A 164, pp. 192-215, (1938).
- [18] M. Sommerfeld, G. Kohnen and M. Rüger, "Some open questions and inconsistencies of Lagrangian particle dispersion models", *proc. Ninth Symp. On Turbulent Shear Flow*, Tokyo, Japan, Paper 5.1, (1993).
- [19] A. Berlemont, M.S. Granicher and G. Gouesbet : Heat and mass transfer coupling between vaporizing droplets and turbulence using a Lagrangian approach. *J. of Heat and Mass Transfer* Vol.38 3023-3034, (1995).
- [20] J. H. Park, Y. Yoon, S. Hwang "Improved Tab-Model for Prediction of Spray Droplet Deformation and Breakup" *J. of atomization and Sprays*, 12, 387-402, (2002).
- [21] T. Crowe, On models for turbulence modulation in fluid-particle flows, *Int. J. Multiphase Flow*, Volume 26, 719-727, (2000).
- [22] S. H. Stårner, J. Gounder, and A. R. Masri, *Com. & Flame*, Vol. 143, pp 420-432, Dec. (2005).
- [23] A. R. Masri and J.D. Gounder, *Proc. of the 6th Mediterranean Com. Symp.*, (2009).
- [24] C. T. Crowe, "Multiphase Flow Handbook", ISBN-10: 0849312809, section 12 page 116 (2005).
- [25] B. Abramzon, W.A. Sirignano, "Approximate theory of a single droplet vaporization in a convective field: Effects of variable properties, Stefan flow and transient liquid heating", *Proceedings of the 1987 ASME/JSME Thermal Engineering Joint Conference*, Honolulu, Hawaii, USA, March 22-27, Vol. 1, pp. 11-18, (1987).
- [26] G. Kohnen, M. Ruger and M. Sommerfeld , Convergence behavior for numerical calculations by the Euler/Lagrange method for strongly coupled phases. In: C.T. Crowe, R. Johnson, A. Prosperetti, M. Sommerfeld and Y. Tsuji, *Editors, Numerical Methods in Multiphase Flows* ASME FED 185, pp. 191-202, (1994).
- [27] A. R. Masri and J.D. Gounder: *Turbulent Spray Flames of Acetone and Ethanol Approaching Extinction*, *Combustion Science and Technology*, Vol.182 (Issues 4-6), pp. 702-715, (2010).
- [28] A. Sadiki, M. Chrigui, J. Janicka and M.R. Maneshkarimi, "Modeling and Simulation of Effects of Turbulence on Vaporization, Mixing and Combustion of Liquid-Fuel Sprays", *J. of Flow Turbulence and Combustion*, 74 pp. 145-167, (2005).